Diffusion Mechanism of Li Argyrodite Solid Electrolytes for Li-Ion Batteries and Prediction of Optimized Halogen Doping

The Effect of Li Vacancies, Halogens, and Halogen Disorder

De Klerk, Niek J J; Roslon, Irek; Wagemaker, Marnix

DOI
10.1021/acs.chemmater.6b03630

Publication date
2016

Document Version
Accepted author manuscript

Published in
Chemistry of Materials

Citation (APA)
De Klerk, N. J. J., Roslon, I., & Wagemaker, M. (2016). Diffusion Mechanism of Li Argyrodite Solid Electrolytes for Li-Ion Batteries and Prediction of Optimized Halogen Doping: The Effect of Li Vacancies, Halogens, and Halogen Disorder. *Chemistry of Materials*, *28*(21), 7955-7963. https://doi.org/10.1021/acs.chemmater.6b03630

Diffusion mechanism of Li-argyrodite solid electrolytes for Li-ion batteries and prediction of optimised halogen doping: the effect of Li-vacancies, halogens, and halogen disorder.

Niek J.J. de Klerk, Irek Rosłoń, and Marnix Wagemaker*

Department of Radiation Science and Technology, Delft University of Technology, Mekelweg 15, 2629JB Delft, The Netherlands

E-mail: m.wagemaker@tudelft.nl

Abstract

Using DFT MD-simulations the origin of the Li-ion conductivity in argyrodite solid electrolytes is investigated. The simulations show that besides Li-ion vacancies in Li_6PS_5Cl and Li_6PS_5Br the influence of halogen atoms on their local surroundings also plays an important role in the Li-ion diffusion. The orders of magnitude difference in Li-ion conductivity between Li_6PS_5Cl and Li_6PS_5I is caused by the distribution of the halogen ions over the available crystallographic sites. This suggests that altering the halogen distribution in Li-argyrodites during synthesis could increase the Li-ion conductivity of these materials. For Li_6PS_5Cl the simulations predict an optimal Cl-distribution of 1:3 over 4a- and 4c-sites, resulting in a Li-ion conductivity two times larger than the currently prepared materials. Based on these results simulations were performed on $Li_5PS_4X_2$ (X = Cl, Br or I), which show Li-ion conductivities similar to Li_6PS_5Cl and Li_6PS_5Br, suggesting that the $Li_5PS_4X_2$ compounds are interesting new compositions for solid state electrolytes.

Introduction

Li-ion batteries are an important technology in the current society, powering laptops, mobile phones, electric cars, etc. However, the use of liquid electrolytes makes current batteries prone to dangerous thermal runaway reactions, igniting the battery[1]. To improve the safety, liquid electrolytes should be replaced by solid state electrolytes, of which several show Li-ion conductivities comparable to liquid electrolytes[2,3]. Besides the improved safety, solid state electrolytes potentially have additional advantages such as an increased voltage stability window, increased energy density due to more efficient packing, and versatility in the battery geometry[2,3]. Lithium argyrodites are a promising family of solid state electrolytes, characterized by the general composition Li_7PnCh_6, where Pn = P or As, and Ch = O, S or Se. By replacing part of the Ch-atoms with halogens (X) the composition Li_6PnCh_5X can be obtained[4], of which Li_6PS_5Cl and Li_6PS_5Br show Li-ion conductivities comparable to liquid electrolytes[5]. Although calculations indicate that the argyrodite structures are unstable[6] a large range of compositions has been synthesised. These include Li-argyrodites containing oxygen[7], arsenic[4], selenium[8], halogens[9], and combinations of these[4]. The highest room temperature Li-ion conductivities are reported for Li_6PS_5Cl and Li_6PS_5Br, reaching up to 10^{-3} S/cm[5,10,11]. However, the related Li_6PS_5I structure shows an orders of magnitude lower conductivity, attributed to the different ordering of I- and Cl-/Br-ions over 4a- and 4c-sites[12]. The Li-ion conductivity of Li_6PO_5Cl and Li_6PO_5Br has been reported to be around 10^{-9} S/cm[7], this is attributed to the 20% smaller lattice constants which drastically reduces the free volume for lithium ion diffusion. Besides a high conductivity the halogen-argyrodites also show excellent electrochemical stability from 0 to 7 V vs. Li/Li^+[10], and a low electronic conductivity on the order of 10^{-10} S/cm[13]. Most argyrodites show a high temperature (HT) and a low temperature (LT) phase[14], but the temperature at which the phase transition occurs strongly depends on the composition[4,15]. Without halogens the HT-phase occurs above 450 K, but halogens stabilise the HT-phase down to 170 K. Since the halogen containing argyrodites show the highest Li-ion conductivities we are primarily interested

in the HT-phase. The HT-phase crystallises in the cubic $F\bar{4}3m$ space group, responsible for the beneficial three dimensional diffusion pathway through the lattice. The excellent electrochemical and thermal stability, high conductivity, facile synthesis[10], the possibility of preparation from solution[16], and cheap starting materials make the halogen-argyrodites an excellent electrolyte candidate for solid state batteries. Recently several groups have reported on solid state batteries using either Li_6PS_5Cl[11,16–19] or Li_6PS_5Br[13,20–22]. Batteries with coulombic efficiencies of 99%[17,19,22] and excellent stability upto 700 cycles[22] have been reported. Recently, solid state NMR measurements of the Li-exchange between argyrodite electrolytes and a Li_2S-cathode has shown that the electrode-electrolyte interface limits the power of these solid state batteries[18]. Despite the increasing amount of research on Li-argyrodites the diffusion mechanism is not yet fully understood. NMR measurements[23] and bond valence calculations[12] have shown that several different jump processes play a role, which together are responsible for the macroscopic Li-ion diffusion. Furthermore, neutron diffraction combined with conductivity measurements has shown that halogen disorder over the 4a- and 4c-sites has a large influence on the Li-ion conductivity[19], but the origin of the increased conductivity is unclear. In a recent work on a Na-ion solid electrolyte[24] we have shown that a better understanding of the diffusion mechanism can give direction to the synthesis of better conducting materials. In this paper we aim to do the same for the Li-argyrodites. The results of density functional theory (DFT) molecular dynamics (MD) simulations performed on a range of argyrodite structures are presented to provide understanding of the Li-ion diffusion in argyrodites. The MD-simulations rationalize the impact of Cl- and Br-doping on the Li-ion conductivity, the role of the halogen disorder is revealed, and guidelines to obtain better Li-ion conducting argyrodites are presented.

Methods

The DFT MD-simulations were performed with VASP[25], using the GGA approximation[26] and the PAW-PBE basis set[27] with a cut-off energy of 280 eV. Given the large unit cell size of 10 Ångstrom all the calculations were performed using one unit cell. During the minimisations a k-point mesh of 2x2x2 was used, which was reduced to 1x1x1 for the MD-simulations. The total simulation time of the MD-simulations was 100 ps., with 2 fs. time-steps, and 2.5 ps. initial equilibration time. Simulations were performed in the NVT ensemble, with temperature scaling after every 1000 time-steps. For all the compositions MD-simulations were performed at 300, 450 and 600 K. As a starting point for the minimisations structures from literature were used if available, otherwise the most similar structure was used. Obtaining the appropriate amount of Li-ions in the unit cell was done by removing one Li-ion from every 48h-site pair, since the small Li-Li distance of 1.9 Ångstrom makes it energetically unfavourable to occupy both 48h-sites in a pair simultaneously. The jump rates were determined by monitoring which crystal sites each Li-ion visits during a MD-simulation, as described in a previous publication[24]. The crystal site-radius was chosen to be as large as possible without causing overlap between neighbouring sites. This results in crystal site-radii of approximately 0.9 Ångstrom, the precise value depending on the unit cell size. Counting the number of jumps between sites (J) gives the mean jump rate (τ) using:

$$\tau = \frac{J}{Nt} \tag{1}$$

where N is the number of Li-ions, and t the simulation time. Based on the jump rate the activation energy (ΔE_A) can be calculated with[28]:

$$\Delta E_A = -kTln(\frac{\tau}{v_0}) \tag{2}$$

where k is Boltzmann's constant, T the temperature in Kelvin, and v_0 the attempt frequency. The jump rate diffusivity (D_J) can be calculated using the Einstein-Smulochowski relation:

$$D_J = \frac{\tau a^2}{2d} \tag{3}$$

where a is the jump distance and d the number of diffusion dimensions (3 in this case). The diffusivity can also be calculated using the mean square displacement (MSD) of the Li-ions during a simulation, commonly known as the tracer diffusivity. The tracer diffusivity (D^*) is calculated using[29]:

$$D^* = \frac{1}{2dN} \sum_{i=1}^{N} \left(\frac{r_i(t)}{dt} \right)^2 \tag{4}$$

where $r_i(t)$ is the displacement of a single Li-ion, and dt is the simulated time. Using the diffusivity (either D_J or D^*) the conductivity (σ) can be determined using the Nernst-Einstein relation[29]:

$$\sigma = \frac{ne^2z^2}{k_BT} D \tag{5}$$

where n is the diffusing particle density, e the elementary electron charge, and z the ionic charge. The conductivity calculated based on D^* and D_J will be referred to as σ^* and σ_J, respectively. To determine the uncertainty in the simulations the standard deviation for all the properties based on the jump rates has been calculated by dividing each simulation into ten parts. Assuming uncorrelated jump processes no equilibration is necessary between the different parts, thus avoiding an increase in the required simulation time.

Results & Discussion

Although several argyrodites are not stable at room temperature in the high temperature (HT) phase, including Li_7PS_6 and Li_7PSe_6, all simulations are performed on the HT-phase of each composition to gain understanding of the influence of the argyrodite composition on the Li-ion conductivity. The high-temperature Li_7PS_6-phase is shown in Figure 1, representing

the cubic unit cell in the $F\bar{4}3m$ (no. 216) space-group where the unit cell parameters are close to 10 Ångstrom for all the experimentally determined structures[4,9,15,30]. The backbone is build up by PS_4-groups centred at 4b-sites, with the remaining sulphur occupying the 4a- and 4c-sites, and the Li-ions occupy 48h-sites surrounding the 4c-sites. Upon substitution of sulphur by halogens, the halogens occupy the 4a- or 4c-sites, whereas the sulphur in the PS_4-groups are not substituted[9]. The Li-ions are distributed over the available 48h-sites, of which approximately 50% are occupied[12]. The existence of pairs of 48h-sites separated by only 1.9 Ångstrom suggests that each pair of 48h-sites is occupied by just one Li-ion[12]. Twelve 48h-sites (6 pairs) surround each 4c-site, which appears as a cage-like Li-ion structure. Besides the 48h-site other crystallographic sites are also suggested to be suitable locations for Li-ions[4], but there is no crystallographic evidence that these sites are occupied. Between the

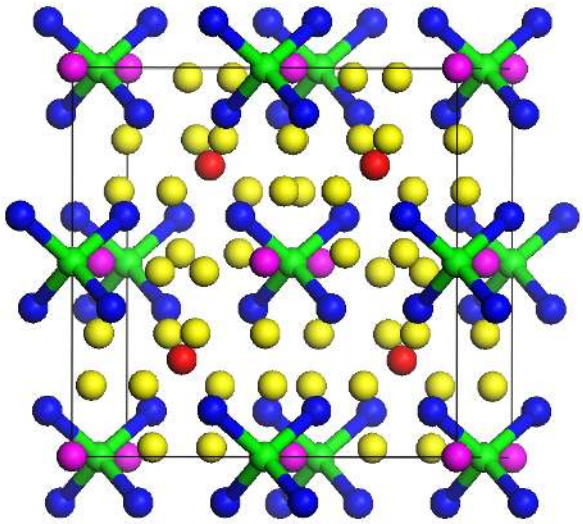

Figure 1: Crystal structure of HT-Li_7PS_6[15]. Colours correspond to; yellow: Li-sites (48h), green: phosphorus, blue: bonded sulphur, pink: 4a-sites, red: 4c-sites

48h-sites in the HT-argyrodite structure three different types of jumps were identified during the MD-simulations. The first type is a jump between the paired 48h-sites over a distance of 1.9 Ångstrom, which we will refer to as a doublet-jump. The second type are the jumps within the cages between different 48h-pairs over a distance of 2.25 Ångstrom, which we will refer to as intracage jumps. The third type are the jumps interconnecting the 4 cages in each

unit cell, for which the distance can vary, which will be referred to as intercage jumps. In order to have Li-ion diffusion pathways throughout the crystal these three jump-types must all occur, and the one with the smallest jump rate will limit the macroscopic diffusion.

Conductivities

The MD-simulations were performed on the HT-phases of the Li_7PS_6, Li_7PSe_6, Li_6PS_5Cl, Li_6PS_5Br and Li_6PS_5I argyrodite compositions to investigate the influence of S versus Se, and the influence of the halide dopants on the Li-ion conductivity. The conductivities from the simulations are shown in Figure 2, the jump rates and activation energies for the three types of jumps are shown in Table S1, S2, and S3 in the supplementary information. For all compositions the intercage jump rate has the lowest frequency, and is therefore used to determine the macroscopic conductivity. In the simulations of Li_6PS_5I and the simulations of Li_7PS_6 and Li_7PSe_6 at 300 K no intercage jumps occurred during the MD-simulations. Only local Li-ion jumps (doublet and intracage) are predicted to occur, and consequentially these compositions showed no macroscopic conductivity on the time-scale of the MD-simulations, as shown in Figure 2. The jump distance used to calculate the conductivity based on the intercage jump frequency, σ_J, is the distance between the centres of the cages, which equals 7.0 Ångstrom. Because the other two jump frequencies are much larger than the intercage jump frequency, the average position of a Li-ion between two intercage jumps is the centre of the cage, and hence intercage jumps effectively take place between the centres of the cages. The MD-simulations predict Li_6PS_5Cl and Li_6PS_5Br to have the highest conductivity, followed by Li_7PS_6 and Li_7PSe_6, and finally Li_6PS_5I, consistent with experiments[12]. The Li-ion conductivities predicted by the MD-simulations are several orders of magnitude larger compared to that measured by impedance spectroscopy. For Li_7PS_6 and Li_7PSe_6 this is caused by the fact that the MD-simulations were performed on the HT-phase, while experiments have been performed on the LT-phase of these compounds[8,14]. The large differences for Li_6PS_5Cl and Li_6PS_5Br may be explained by the influence of grain boundaries on impedance spectroscopy

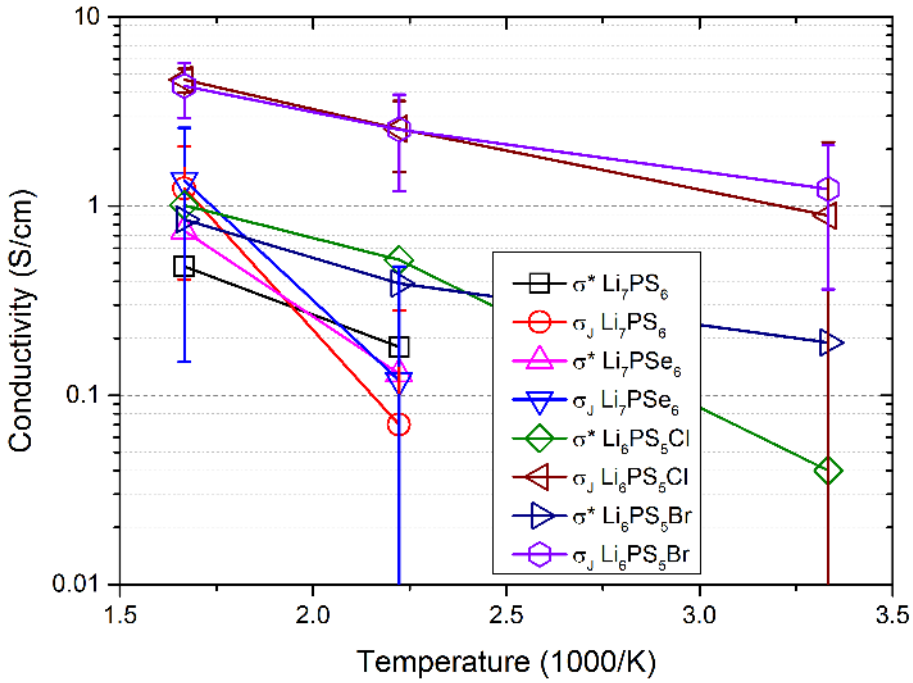

Figure 2: Arrhenius plot of the conductivities from MD-simulations based on the intercage jump frequency, σ_J, and the MSD, σ^*.

results, which probes charge transport over tens of nanometres, and since grain boundaries appear to limit the macroscopic conductivity[18], impedance spectroscopy effectively measures the lower limit for Li-ion conductivity in argyrodites. Whereas in the MD-simulations a perfectly crystalline structure is assumed, effectively giving an upper limit for the Li-ion conductivity. Direct measurement of the local Li-ion mobility inside Li-argyrodite crystals with ^{7}Li NMR relaxation measurements[18,23] results in conductivities having the same order of magnitude as the present MD-simulations, validating the use of DFT MD-simulations to predict the Li-ion dynamics in the argyrodite structures. The difference between the values of σ_J and σ^* from the MD-simulations is caused by 'back and forth' jumps, which contribute to σ_J, but cancel each other in σ^*. As a consequence the conductivity based on the jump rates should be larger than that based on the MSD, and hence the correlation factor $f = \frac{D^*}{D_J}$ [31] is smaller than 1. For Li_6PS_5Br and Li_6PS_5Cl the correlation factor is below 0.2 for all the simulated temperatures, indicating that a significant amount of back and forth

jumps occur in these compounds. In Li_7PS_6 and Li_7PSe_6 the correlation factor strongly changes with temperature, probably caused by the small number of jumps per Li-ion, which is reflected in the large error bars for σ_J. The small number of jumps per Li-ion makes it unlikely that a Li-ion will perform multiple jumps, thus back and forth jumps are not very likely to occur. To obtain a reliable value for the correlation factor in these compositions more jumps per Li-ion must be sampled, however, this would require much longer simulation times outside the scope of this study. It has been reported that increasing the lattice volume of solid electrolytes, by introducing atoms with larger ionic radii, can significantly influence the Li-ion conductivity[2]. In argyrodites the larger ionic radius of bromide compared to chloride leads to an increase in the cubic lattice parameter, amounting to 0.13 Ångstrom[12], and replacing S by Se leads to an increase of 0.48 Ångstrom[15]. Comparison of the conductivities from the MD-simulations of Li_7PS_6 with Li_7PSe_6 and Li_6PS_5Cl with Li_6PS_5Br does not suggest a significant effect of the ionic radius on the conductivity in the argyrodite structure. However, large differences in the doublet and intracage jump rates are observed for the different compositions (see Tables S1, S2, and S3 in the S.I.), hence the ionic radius of the ions appears to affect the Li-ion dynamics. However, the intercage jump rates, which determine the macroscopic conductivity, in Li_7PSe_6 and Li_6PS_5Br are similar to those in Li_7PS_6 and Li_6PS_5Cl, respectively. Therefore the lattice volume per Li-ion does not have a significant influence on the macroscopic Li-ion conductivity in argyrodites. To understand what causes the differences in Li-ion conductivity between the Li-argyrodites, the Li-density during MD-simulations is shown for Li_7PS_6, Li_6PS_5Cl and Li_6PS_5I in Figure 3. The Li-densities of Li_7PSe_6 and Li_6PS_5Br, shown in Figure S1 in the supplementary information, are very similar to that of Li_7PS_6 and Li_6PS_5Cl, respectively. The Li-ion densities in Figures 3 and S1 all show the four cage-like structures in which the Li-ions reside surrounding the 4c-sites. For Li_6PS_5I the Li-density clearly shows why this is a poor Li-ion conductor. The high Li-ion density regions reflect high mobility between pairs of 48h-sites, the doublet jumps, which are also observed by XRD[4] and NMR experiments[30]. However, no diffusion

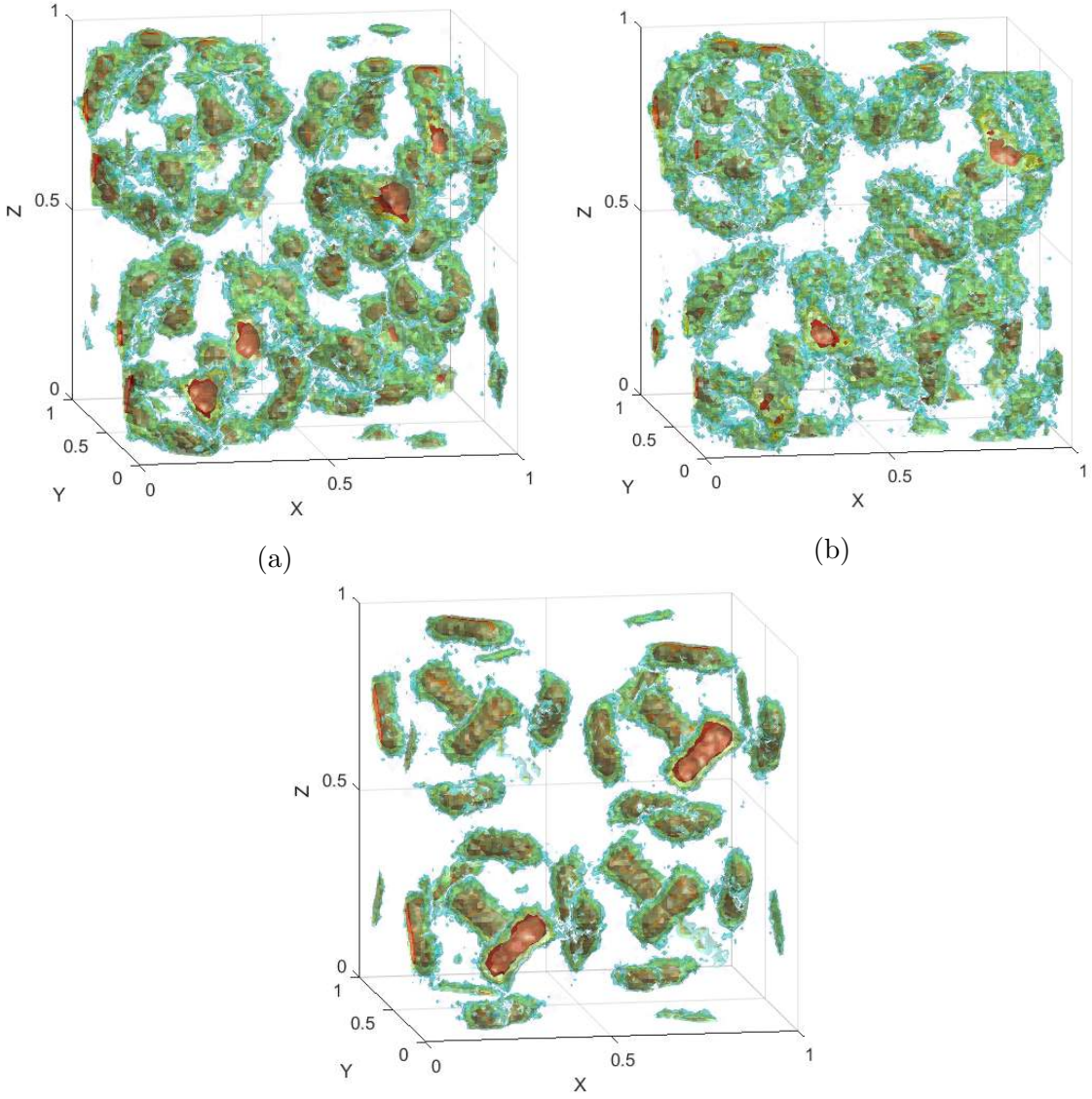

Figure 3: Li-ion density in the argyrodite unit cell during MD-simulations at 450 K of (a) Li_7PS_6, (b) Li_6PS_5Cl and (c) Li_6PS_5I. Red indicates high Li-ion density, followed by yellow, green, and blue representing lower densities.

paths between the pairs of 48h-sites are visible, and the Li-ions in Li_6PS_5I thus only display local mobility, explaining its low macroscopic Li-ion diffusion. In the other compositions the regions with high Li-ion densities are connected to neighbouring high density regions within a cage, although connections between different cages are not clearly visible. However, there are subtle differences between the Li-ion densities in Li_7PS_6 and Li_6PS_5Cl. In Figure 3 the Li-ions in Li_7PS_6 appear to be more localized, as observed by the larger maxima in the Li-ion density. In Li_6PS_5Cl the maxima are smaller, and the Li-ion density is more spread out over the Li-ion positions, indicating that the Li-ions are moving around more rapidly inside the cages. In Figure S1 (in the S.I.) similar behaviour is visible in Li_7PSe_6 and Li_6PS_5Br. The origin of the large differences in macroscopic conductivity in Figure 3 are easier to analyse by the jump statistics schematically shown for Li_7PS_6, Li_6PS_5Cl, and Li_6PS_5I in Figure 4 (and Figure S2 in the S.I. for Li_7PSe_6 and Li_6PS_5Br). In Li_6PS_5I doublet jumps occur very frequently, as already visible in the Li-ion density in Figure 3. Furthermore, only a few intracage jumps occur, and not a single intercage jump takes place during the MD-simulation, thus unambiguously revealing why Li_6PS_5I is a poor Li-ion conductor. In all other compositions the frequent doublet and intracage jumps clearly reveal the cage structure formed by the diffusing Li-ions around the 4c-sites. But only in Li_6PS_5Cl and Li_6PS_5Br a significant number of intercage jumps occurs, making macroscopic Li-ion diffusion possible. For Li_6PS_5Cl ^{7}Li NMR relaxation experiments have measured jump rates of approximately $1*10^9$ sec^{-1} at 350 K[18]. The predicted jump rates at 300 K are an order of magnitude larger as the results from the NMR experiments, but there is a large uncertainty in the jump rates at 300 K due to the limited amount of jumps occurring during the simulation time. However, extrapolating the jump rate conductivities of Li_6PS_5Cl at 450 and 600 K towards 350 K, using the activation energies predicted by the MD-simulations, does show good agreement with the NMR results[18]. Using impedance spectroscopy activation energies between 0.16 and 0.56 eV have been reported for Li_6PS_5X (X = Cl, Br or I)[12,14,19], strongly depending on the synthesis[19] and measurement procedure[14]. NMR experiments report activation energies of

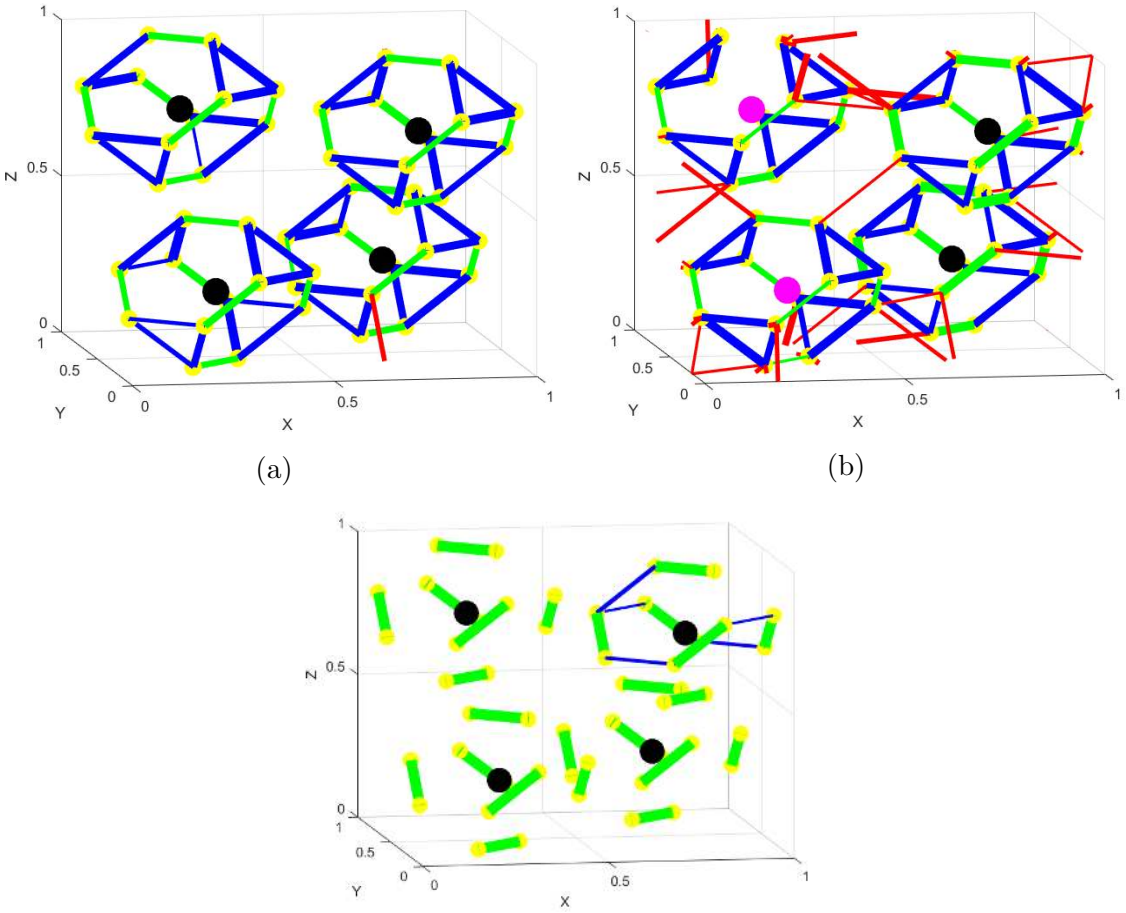

(a) (b)

(c)

Figure 4: Jump statistics plots from MD-simulations at 450 K of (a) Li_7PS_6, (b) Li_6PS_5Cl and (c) Li_6PS_5I. The lines represent the three different types of jumps; green: doublet, blue: intracage, red: intercage, thicker lines represent larger jump rates. The coloured spheres indicate; black: S at 4c, pink: Cl at 4c, yellow: Li-ion sites (48h).

0.08 and 0.09 for short range and 0.20 and 0.29 eV for long range diffusion in Li_6PS_5Br[23] and Li_6PS_5Cl[18], respectively. Using Equation 2, with a typical attempt frequency[31] of $1 * 10^{13}$, the MD-simulations predict activation energies in Li_6PS_5Cl and Li_6PS_5Br of 0.10 to 0.14 eV for doublet- and intracage-jumps, and 0.20 to 0.25 eV for intercage jumps, comparable to the experimental results from NMR. The energy barriers for short range jumps resulting from the present MD-simulations are similar to those from bond-valence calculations[12,19], which report activation barriers between 0.10 and 0.20. For intercage jumps bond valence calculations report activation energies between 0.30 and 0.35, slightly above the results from the current MD-simulations and NMR measurements. Comparing the jump rates and activation energies of the different types of jumps clearly shows that the intercage jumps are rate limiting, and hence determine the macroscopic Li-ion conductivity in the argyrodite Li-ion electrolytes. In all the experimentally reported argyrodite compositions the intercage jump rate is at least 5 times smaller than the jump rates of the other jump types during the MD-simulations. Although all three types of jumps are necessary for macroscopic diffusion, this shows that to achieve higher Li-ion conductivities in argyrodites the intercage jump rate should be increased in the first place.

Vacancies

The differences in the intercage jump rates illustrates why the Li-ion conductivity in Li_6PS_5Cl is much higher than in Li_7PS_6, but does not explain the origin of the larger intercage jump rate. The most obvious explanation is that replacing S^{2-} by Cl^{1-} results in charge compensating Li-ion vacancies that induce the larger Li-ion conductivity. To test this explanation simulations were performed on the artificial Li_6PS_6 and Li_7PS_5Cl compositions, the results of which are shown in Figure 5. If only the Li-ion vacancies in Li_6PS_5Cl are responsible for the high conductivity the Li_6PS_6 composition should result in a high Li-ion conductivity by frequent intercage jumps, whereas in Li_7PS_5Cl the decreased amount of vacancies should result in significantly less intercage jumps. However, in Figure 5 similar behaviour is visible

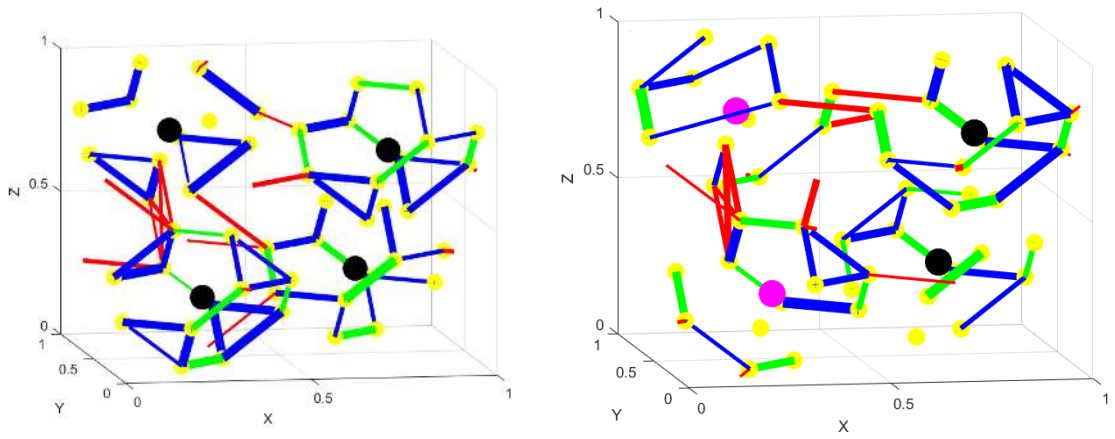

(a) (b)

Figure 5: Jump statistics plots from MD-simulations at 450 K of (a) Li_6PS_6, and (b) Li_7PS_5Cl. The lines represent the three different types of jumps; green: doublet, blue: intracage, red: intercage, thicker lines represent larger jump rates. The coloured spheres indicate; black: S at 4c, pink: Cl at 4c, yellow: Li-ion sites (48h).

for the Li_6PS_6 and Li_7PS_5Cl compositions. Around the 4c-sites cages are visible in which the Li-ions diffuse, which are interconnected by intercage jumps. Although Li_6PS_6 and Li_7PS_5Cl show significant differences in the intracage and doublet jump rates, the rate limiting intercage jump rates are similar. These results indicate that Li-ion vacancies and substituting S with Cl changes the jump rates significantly, and both are responsible for increasing the Li-ion conductivity in Li_6PS_5Cl. It is obvious that increasing the amount of vacancies, to a certain degree, will enhance the Li-ion diffusivity, but understanding the impact of Cl-doping requires a more detailed analysis. The question is what change in local environment, caused by replacing S with Cl, is responsible for the improved conductivity. To bring forward the difference in the local environment of Cl- and S-ions the radial distribution functions (RDF's) around the atoms located on the 4c- and 4a-sites were determined. The RDF's in Figures 6 and S3 (in the S.I.) reflect the Li-ion density as a function of distance with respect to the S- or Cl-ion on the 4c-site (4a-site in Figure S3), clearly reflecting the Li-ion density due to the Li-ions in the cage by a peak around 2.5 Ångstrom. In Figure 6 a significant difference in Li-ion density is observed when comparing the RDF's around the Cl- and S-ions at 4c-

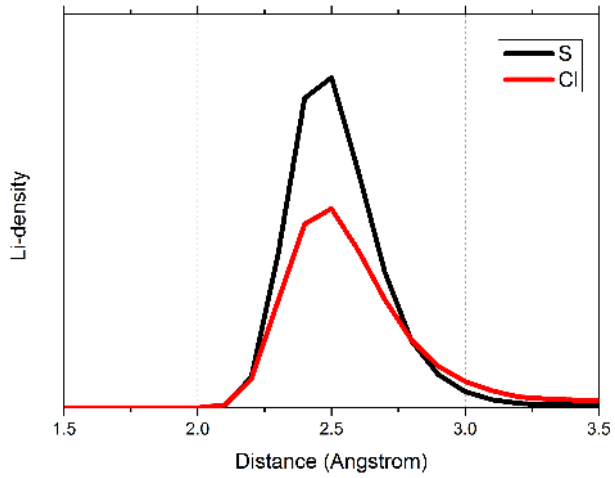

Figure 6: Radial distribution functions representing the Li-density as a function of distance around the Cl- and S-ions at the 4c-sites in Li_6PS_5Cl during the MD-simulation at 450 K.

sites. Although the peak width and position are equal for Cl and S, the Li-density around the S-ions is significantly larger. Integrating the Li-density upto 3.5 Ångstrom shows that on average there are 5 Li-ions in the cage surrounding the Cl-ions and 7 Li-ions surround the S-ions. A similar Li-distribution is observed for Cl-ions at 4a-sites, as shown in the supplementary information (Figure S3). Therefore, (on average) there is always an empty doublet of 48h-sites near the Cl-ions, facilitating intercage jumps. This can be explained by the lower ionic charge of the Cl-ions compared to S-ions, which is charge compensated by the extra vacancies on the Li-sites near Cl-ions. At all the simulated temperatures a similar Li-distribution is seen in Li_6PS_5Cl and Li_6PS_5Br, indicating that a 5-7 Li-distribution over the cages is more stable as a 6-6 Li-distribution when halogens are present. These results also suggest that the calculated stability of the argyrodites[6] may be strongly influenced by the Li-ion distribution (induced by the halogens). Given the large configurational space on the Li-ion sub-lattice it is beyond the scope of this paper to consider the stability dependence on the Li-ion configuration.

Halogen disorder

The impact of vacancies on the Li-ion jumps does not explain the orders of magnitude difference in conductivity between Li_6PS_5Cl and Li_6PS_5I. It has been proposed that the difference in conductivity is caused by the fact that I-ions only occupy the 4a-sites, whereas Cl-ions show disorder, being distributed over the 4a- and 4c-sites[12]. The 4a- and 4c-sites represent Cl-ions located outside and inside the cages, respectively. Furthermore, experiments have shown that increasing the Cl-occupancy of 4c-sites can significantly increase the Li-ion conductivity in Li_6PS_5Cl[19]. To validate whether the disorder of halogen-ions over the 4a- and 4c-site is responsible for the high conductivity in Li_6PS_5Cl and Li_6PS_5Br in comparison to Li_6PS_5I, simulations were performed with different distributions of Cl-ions over the 4a- and 4c-sites in a unit cell of Li_6PS_5Cl. Figure 7 shows that the position of the Cl-ions has a

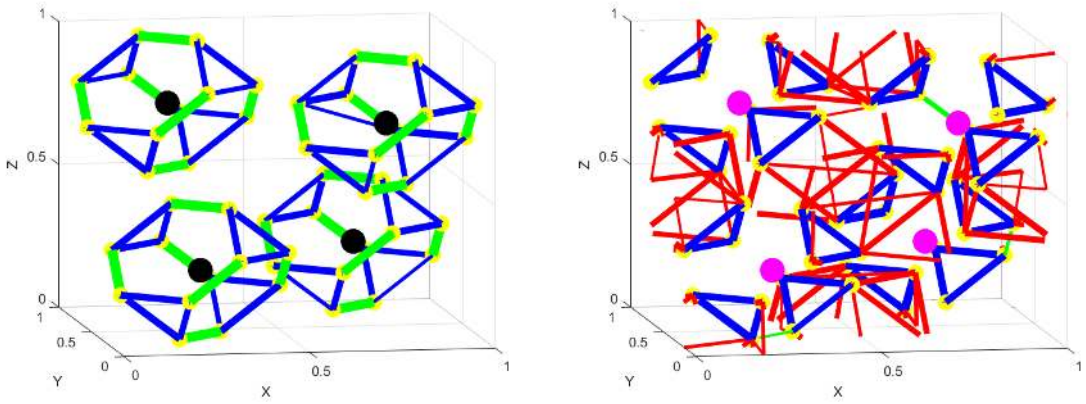

(a) (b)

Figure 7: Jump statistics plots from MD-simulations at 450 K of Li_6PS_5Cl with all chloride (a) on 4a (outside the cages) and (b) on 4c (inside the cages). The lines represent the three different types of jumps; green: doublet, blue: intracage, red: intercage, thicker lines represent larger jump rates. The coloured spheres indicate; black: S at 4c, pink: Cl at 4c, yellow: Li-ion sites (48h).

profound impact on the jump rates, and thus on the conductivity. When all the Cl-ions are located at 4a-sites (similar to I-ions in Li_6PS_5I) no intercage jumps occur during the MD-simulation. Placing all the Cl-ions at the 4c-sites also leads to a low Li-diffusivity, however, not because of the intercage jump rate. In contrast, the Cl-ions on the 4c-sites induce a

very high intercage jump rate, but the doublet jump rate decreases drastically and becomes rate limiting, thereby causing the intercage jumps to become a local motional process. In this case the Li-ion mobility is limited by the doublet jumps, which thus determines the macroscopic Li-ion conductivity in this structure. These simulations demonstrate that distributing the halogens over the 4a- and 4c-sites, referred to as halogen disorder, is essential for inducing high macroscopic Li-ion diffusion. It also explains why crystalline Li_6PS_5I, in which all I-ions occupy 4a-sites, shows a Li-ion diffusivity orders of magnitude smaller than crystalline Li_6PS_5Cl[12]. In Figure 8 the jump rates of the different jump processes are plotted as a function of Cl-occupancy of the 4c-sites, showing a clear relation between the jump rates and the Cl-distribution. The doublet jump rate decreases with increasing Cl-occupancy of

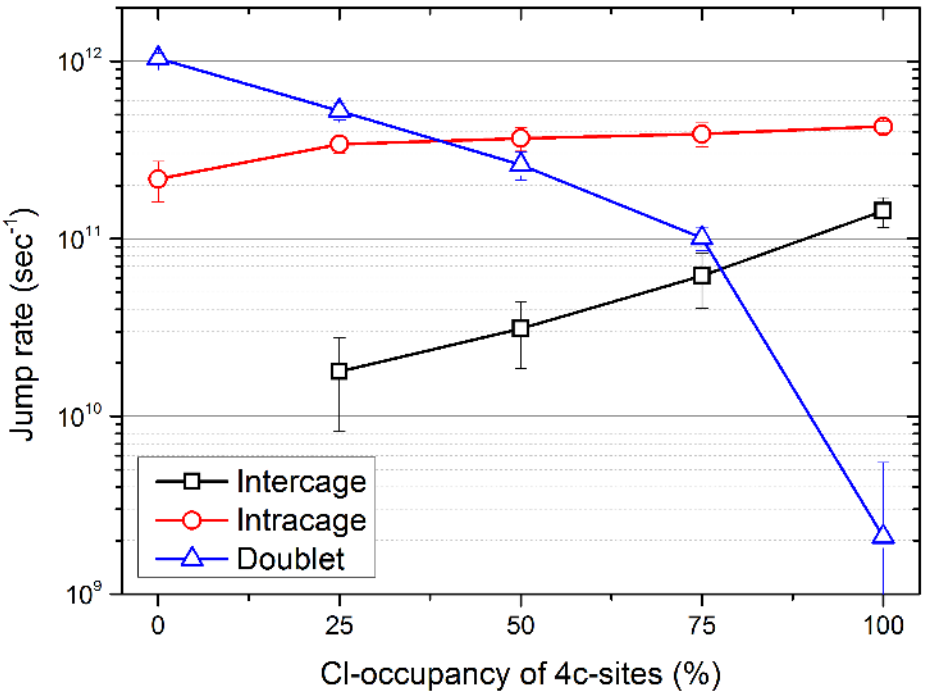

Figure 8: Jump rates as a function of Cl-occupancy of 4c-sites in Li_6PS_5Cl from MD-simulations at 450 K.

the 4c-sites, while the intercage jump rate increases, and the intracage jump rate is nearly constant. To obtain the highest possible Li-ion conductivity the limiting jump rate should be as high as possible, which in Li_6PS_5Cl can be the doublet or intercage jumps, depending on

the Cl-ordering over 4a- and 4c-sites. The results in Figure 8 indicate that the highest Li-ion conductivity can be obtained when $\frac{3}{4}$ of the 4c-sites (and $\frac{1}{4}$ of the 4a-sites) are occupied by Cl-ions. At this distribution the lowest jumps frequency is maximised, showing a limiting jump rate two times larger compared to when the Cl-ions are evenly distributed over 4a- and 4c-sites. It has been shown that the disorder of Cl in argyrodites can be tailored by heat treatment[19], therefore optimising the synthesis conditions to obtain a 1:3 Cl-distribution over 4a- and 4c-sites, is at present predicted to double the Li-ion conductivity in Li_6PS_5Cl. Note that the different halogens influence the rate of each jump type differently (see Tables S1, S2, and S3 in the S.I.), and therefore the 4a-4c distribution for Li_6PS_5Br and Li_6PS_5I which maximises the Li-ion conductivity will probably differ from the optimal 4a-4c distribution of Li_6PS_5Cl.

$Li_5PS_4X_2$

The results of the MD-simulations indicate that introducing halogens in the argyrodite structure increases the Li-ion conductivity, under the condition that the halogen ions are distributed over the 4a- and 4c-sites. A logical step to increase the conductivity further would be to introduce a larger amount of halogens, and consequently also more Li-vacancies, giving the composition $Li_5PS_4X_2$ (X = Cl, Br or I). The similar stability of Li_6PS_5X and $Li_5PS_4X_2$ compounds[6] suggests that synthesis of these compounds should be possible. The larger amount of Li-vacancies would make Li-diffusion easier, although the jump rates in Figure 8 suggest that Cl-ion occupying all of the 4a- and 4c-sites might hinder intercage and doublet jumps. To determine whether introducing more halogens is beneficial for the Li-ion conductivity simulations were performed on $Li_5PS_4Cl_2$, $Li_5PS_4Br_2$, and $Li_5PS_4I_2$, the results of which are shown in Figure 9. During the MD-simulations macroscopic Li-ion conductivity is observed in all the $Li_5PS_4X_2$ compositions, except for $Li_5PS_4I_2$ at 300 K. While simulations of Li_6PS_5Cl in which the 4a- or 4c-sites are completely occupied display low limiting jump rates, as shown in Figure 8, the combination of completely occupied 4a- and 4c-sites in

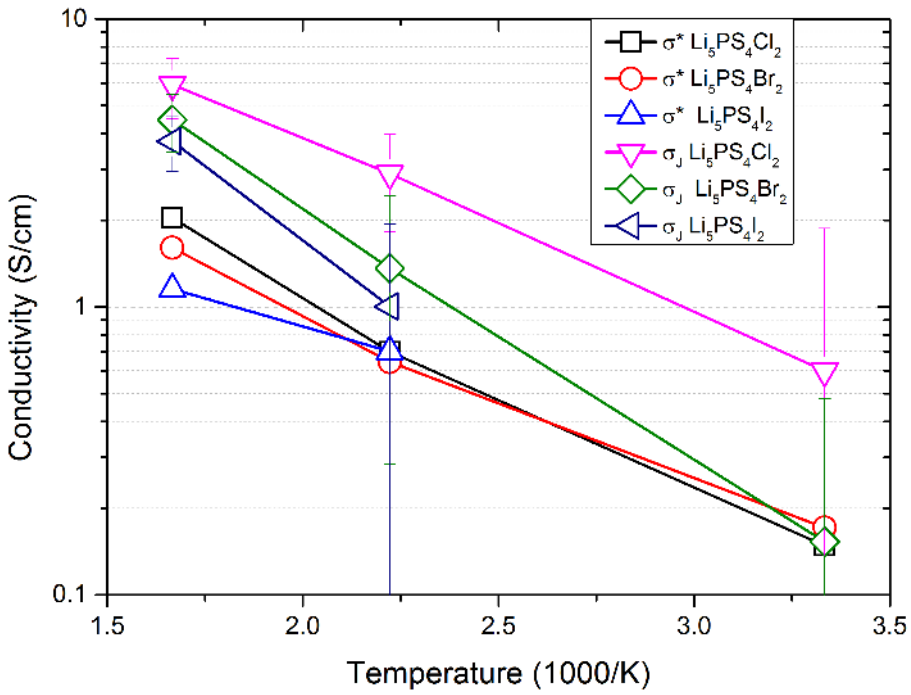

Figure 9: Arrhenius plot of the conductivities of $Li_5PS_4X_2$ compounds from MD-simulations based on the intercage jump frequency, σ_J, and the MSD, σ^*.

$Li_5PS_4Cl_2$ performs well. Apparently the complete Cl-occupancy of 4a- and 4c-sites does not hinder the jump rates, but the 4a- or 4c-sites being unoccupied by Cl-ions seems to decrease certain jump rates in Li_6PS_5Cl. This is an additional proof that the combination of occupied 4a- and 4c-sites is essential for macroscopic conductivity in Li-argyrodites. With iodine occupying 4a- and 4c-sites at 450 and 600 K $Li_5PS_4I_2$ shows a conductivity comparable to $Li_5PS_4Cl_2$ and $Li_5PS_4Br_2$, whereas Li_6PS_5I does not show any macroscopic diffusion at these temperatures. Therefore, to improve the Li-ion conductivity in $Li_{7-x}PS_{6-x}I_x$ a fraction of the I-ions should occupy the 4c-sites. Increasing the I-content above $x = 1$ implies that some of the I-ions will occupy the 4c-sites, which is suggested to be a promising strategy to increase the Li-ion conductivity in $Li_{7-x}PS_{6-x}I_x$. For $Li_5PS_4Cl_2$ and $Li_5PS_4Br_2$ the conductivities are similar to those of Li_6PS_5Cl and Li_6PS_5Br. Although increasing the halogen composition does not significantly alter the Li-ion conductivity, $Li_5PS_4Cl_2$ and $Li_5PS_4Br_2$ may be interesting as solid state electrolytes because other properties of these compositions might

be more favourable than those of Li_6PS_4Cl and Li_6PS_4Br. For instance, it is not unlikely that replacing the non-bonded S^{2-} by Cl^- or Br^- will increase the stability versus oxygen and moisture of the argyrodite crystals, making these halogen rich compositions potentially more suitable for application as a solid state electrolyte.

Conclusions

Using DFT MD-simulations the origin of the Li-ion conductivity in argyrodite solid electrolytes is investigated. Although halogen replacement of sulphur introduces Li-vacancies by charge compensation, the distribution of the halogens over the available sites is equally important. The halogen distribution determines the distribution of Li-vacancies, which is decisive in how the higher local Li-ion diffusivity translates into a higher macroscopic Li-ion conductivity. Halogen substitution on each of the two possible sulphur sites induces a higher jump frequency of a different Li-ion jump process, whereas all three distinct jump processes are required for macroscopic conductivity. This explains why a distribution of the halogens over the two available sites is required for high Li-ion conductivities. The simulations suggest that the Li-ion conductivity can be increased by optimising the halogen distribution over the 4a- and 4c-sites, and by increasing the halogen content in Li-argyrodites, where the latter may have the additional advantage of being more stable versus air and moisture.

Supporting Information

Conductivities, jump rates and activation energies from all the MD-simulations, jump statistics plots and Li-density plots of Li_7PSe_6 and Li_6PS_5Br, and RDF of 4a-sites in Li_6PS_5Cl.

Acknowledgements

Financial support from the Advanced Dutch Energy Materials (ADEM) program of the Dutch Ministry of Economic Affairs, Agriculture and Innovation is gratefully acknowledged. The research leading to these results has received funding from the European Research Council under the European Union's Seventh Framework Programme (FP/2007-2013)/ERC Grant Agreement nr. [307161] of M.W.

References

(1) Roth, E.; Orendorff, C. How electrolytes influence battery safety. *Electrochem. Soc. Interface* **2012**, *21*, 45–49.

(2) Bachman, J. C.; Muy, S.; Grimaud, A.; Chang, H. H.; Pour, N.; Lux, S. F.; Paschos, O.; Maglia, F.; Lupart, S.; Lamp, P.; Giordano, L.; Shao-Horn, Y. Inorganic Solid-State Electrolytes for Lithium Batteries: Mechanisms and Properties Governing Ion Conduction. *Chem. Rev.* **2016**, *116*, 140–62.

(3) Takada, K. Progress and prospective of solid-state lithium batteries. *Acta Mater.* **2013**, *61*, 759–770.

(4) Kong, S. T.; Deiseroth, H. J.; Reiner, C.; Gun, O.; Neumann, E.; Ritter, C.; Zahn, D. Lithium argyrodites with phosphorus and arsenic: order and disorder of lithium atoms, crystal chemistry, and phase transitions. *Chemistry* **2010**, *16*, 2198–206.

(5) Rao, R. P.; Adams, S. Studies of lithium argyrodite solid electrolytes for all-solid-state batteries. *Phys. Status Solidi A* **2011**, *208*, 1804–1807.

(6) Chen, H. M.; Maohua, C.; Adams, S. Stability and ionic mobility in argyrodite-related lithium-ion solid electrolytes. *Phys. Chem. Chem. Phys.* **2015**, *17*, 16494–16506.

(7) Kong, S.-T.; Deiseroth, H.-J.; Maier, J.; Nickel, V.; Weichert, K.; Reiner, C. Li_6PO_5Br and Li_6PO_5Cl: The first Lithium-Oxide-Argyrodites. *Z. Anorg. Allg. Chem.* **2010**, *636*, 1920–1924.

(8) Epp, V.; Gun, O.; Deiseroth, H. J.; Wilkening, M. Long-range Li^+ dynamics in the lithium argyrodite Li_7PSe_6 as probed by rotating-frame spin-lattice relaxation NMR. *Phys. Chem. Chem. Phys.* **2013**, *15*, 7123–32.

(9) Deiseroth, H. J.; Kong, S. T.; Eckert, H.; Vannahme, J.; Reiner, C.; Zaiss, T.; Schlosser, M. Li_6PS_5X: a class of crystalline Li-rich solids with an unusually high Li^+ mobility. *Angew. Chem. Int. Ed.* **2008**, *47*, 755–8.

(10) Boulineau, S.; Courty, M.; Tarascon, J.-M.; Viallet, V. Mechanochemical synthesis of Li-argyrodite Li_6PS_5X (X=Cl, Br, I) as sulfur-based solid electrolytes for all solid state batteries application. *Solid State Ionics* **2012**, *221*, 1–5.

(11) Yu, C.; van Eijck, L.; Ganapathy, S.; Wagemaker, M. Synthesis, structure and electrochemical performance of the argyrodite Li_6PS_5Cl solid electrolyte for Li-ion solid state batteries. *Electrochimica Acta* **2016**, *215*, 93–99.

(12) Rayavarapu, P. R.; Sharma, N.; Peterson, V. K.; Adams, S. Variation in structure and Li^+-ion migration in argyrodite-type Li_6PS_5X (X = Cl, Br, I) solid electrolytes. *J. Solid State Electrochem.* **2011**, *16*, 1807–1813.

(13) Stadler, F.; Fietzek, C. Crystalline Halide Substituted Li-Argyrodites as Solid Electrolytes for Lithium Secondary Batteries. *ECS Transactions* **2010**, *25*, 177–183.

(14) Deiseroth, H.-J.; Maier, J.; Weichert, K.; Nickel, V.; Kong, S.-T.; Reiner, C. Li_7PS_6 and Li_6PS_5X (X: Cl, Br, I): Possible Three-dimensional Diffusion Pathways for Lithium Ions and Temperature Dependence of the Ionic Conductivity by Impedance Measurements. *Z. Anorg. Allg. Chem.* **2011**, *637*, 1287–1294.

(15) Kong, S. T.; Gun, O.; Koch, B.; Deiseroth, H. J.; Eckert, H.; Reiner, C. Structural characterisation of the Li argyrodites Li_7PS_6 and Li_7PSe_6 and their solid solutions: quantification of site preferences by MAS-NMR spectroscopy. *Chemistry* **2010**, *16*, 5138–47.

(16) Yubuchi, S.; Teragawa, S.; Aso, K.; Tadanaga, K.; Hayashi, A.; Tatsumisago, M. Preparation of high lithium-ion conducting Li_6PS_5Cl solid electrolyte from ethanol solution for all-solid-state lithium batteries. *Journal of Power Sources* **2015**, *293*, 941–945.

(17) Boulineau, S.; Tarascon, J.-M.; Leriche, J.-B.; Viallet, V. Electrochemical properties of all-solid-state lithium secondary batteries using Li-argyrodite Li_6PS_5Cl as solid electrolyte. *Solid State Ionics* **2013**, *242*, 45–48.

(18) Yu, C.; Ganapathy, S.; de Klerk, N. J. J.; Roslon, I.; van Eck, E. R.; Kentgens, A. P.; Wagemaker, M. Unravelling Li-Ion Transport from Picoseconds to Seconds: Bulk versus Interfaces in an Argyrodite Li_6PS_5Cl-Li_2S All-Solid-State Li-Ion Battery. *J. Am. Chem. Soc.* **2016**, *138*, 11192–201.

(19) Rao, R. P.; Sharma, N.; Peterson, V. K.; Adams, S. Formation and conductivity studies of lithium argyrodite solid electrolytes using in-situ neutron diffraction. *Solid State Ionics* **2013**, *230*, 72–76.

(20) Chen, M.; Adams, S. High performance all-solid-state lithium/sulfur batteries using lithium argyrodite electrolyte. *J. Solid State Electrochem.* **2014**, *19*, 697–702.

(21) Chen, M.; Prasada Rao, R.; Adams, S. The unusual role of Li_6PS_5Br in all-solid-state CuS/Li_6PS_5Br/In–Li batteries. *Solid State Ionics* **2014**, *268*, 300–304.

(22) Chen, M.; Yin, X.; Reddy, M. V.; Adams, S. All-solid-state MoS_2/Li_6PS_5Br/In–Li batteries as a novel type of Li/S battery. *J. Mater. Chem. A* **2015**, *3*, 10698–10702.

(23) Epp, V.; Gün, Ö.; Deiseroth, H.-J.; Wilkening, M. Highly Mobile Ions: Low-Temperature NMR Directly Probes Extremely Fast Li^+ Hopping in Argyrodite-Type Li_6PS_5Br. *J. Phys. Chem. Lett.* **2013**, *4*, 2118–2123.

(24) de Klerk, N. J. J.; Wagemaker, M. Diffusion Mechanism of the Sodium-Ion Solid Electrolyte Na_3PS_4 and Potential Improvements of Halogen Doping. *Chem. Mater.* **2016**, *28*, 3122–3130.

(25) Kresse, G.; Hafner, J. Ab initio molecular dynamics for liquid metals. *Phys. Rev. B* **1993**, *47*, 558–561.

(26) Perdew, J. P.; Burke, K.; Ernzerhof, M. Generalized Gradient Approximation Made Simple. *Phys. Rev. Lett.* **1996**, *77*, 3865–3868.

(27) Blöchl, P. E. Projector augmented-wave method. *Phys. Rev. B* **1994**, *50*, 17953–17979.

(28) Vineyard, G. H. Frequency factors and isotope effects in solid state rate processes. *J. Phys. Chem. Solids* **1957**, *3*, 121–127.

(29) Friauf, R. J. Correlation Effects for Diffusion in Ionic Crystals. *J. Appl. Phys.* **1962**, *33*, 494–505.

(30) Pecher, O.; Kong, S. T.; Goebel, T.; Nickel, V.; Weichert, K.; Reiner, C.; Deiseroth, H. J.; Maier, J.; Haarmann, F.; Zahn, D. Atomistic characterisation of Li^+ mobility and conductivity in $Li_{(7-x)}PS_{(6-x)}I_x$ argyrodites from molecular dynamics simulations, solid-state NMR, and impedance spectroscopy. *Chemistry* **2010**, *16*, 8347–54.

(31) Van der Ven, A.; Ceder, G.; Asta, M.; Tepesch, P. D. First-principles theory of ionic diffusion with nondilute carriers. *Phys. Rev. B* **2001**, *64*, 184307.

Table of Contents figure